Towards Quantifying the Chemical Sensitivity of Nuclear Spin Surface Relaxivity in Mesoporous Media

Shuang Dong[a,b], Libin Liu[a], Nicholas N. A. Ling[a], Eric F. May[a], Michael L. Johns[a] and Neil Robinson[a,*]

[a]*Department of Chemical Engineering, The University of Western Australia, Perth, WA 6009, Australia*

[b]*Key Laboratory of Ocean Energy Utilization and Energy Conservation of Ministry of Education, Dalian University of Technology, Dalian 116024, China*

***Corresponding Author:**
Dr Neil Robinson
Forrest Fellow
The University of Western Australia

Postal Address:
Department of Chemical Engineering
The University of Western Australia
35 Stirling Highway (M050)
Perth WA 6009
Australia

Email: neil.robinson@uwa.edu.au

Fluid Science and Resources Research Group: www.fsr.ecm.uwa.edu.au

ORCID:

Shuang Dong	0000-0002-1094-8175
Libin Liu	0000-0002-5387-7098
Nicholas N. A. Ling	0000-0003-3396-7704
Eric F. May	0000-0001-5472-6921
Michael L. Johns	0000-0001-7953-0597
Neil Robinson	0000-0002-0893-2190

Abstract

Low-field nuclear magnetic resonance (NMR) relaxation is a promising non-invasive technique for characterizing solid-liquid interactions within functional porous materials. However, the ability of the solid-liquid interface to enhance adsorbate relaxation rates, known as the surface relaxivity, in the case of different solvents and reagents involved in various chemical processes has yet to be evaluated in a quantitative manner. In this study, we systematically explore the surface relaxation characteristics of ten liquid adsorbates (cyclohexane, acetone, water, and seven alcohols, including ethylene glycol) confined within mesoporous silicas with pore sizes between 6 nm and 50 nm using low-field (12.7 MHz) two-dimensional ^{1}H $T_1 - T_2$ relaxation measurements. Functional group specific relaxation phenomena associated with the alkyl and hydroxyl groups of the confined alcohols are clearly distinguished; we report the dependence of both longitudinal (T_1) and transverse (T_2) relaxation rates of these ^{1}H-bearing moieties on pore surface-to-volume ratio, facilitating the quantification and assignment of surface relaxivity values to specific functional groups within the same adsorbate molecule for the first time. We further demonstrate that alkyl group transverse surface relaxivities correlate strongly with the alkyl/hydroxyl ratio of the adsorbates assessed, providing evidence for a simple, quantitative relationship between surface relaxivity and interfacial chemistry. Overall, our observations highlight potential pitfalls in the application of NMR relaxation for the evaluation of pore size distributions using hydroxylated probe molecules, and provide motivation for the exploration of nuclear spin relaxation measurements as a route to adsorbate identity within functional porous materials.

Keywords: Adsorption, porous materials, NMR relaxation, surface relaxivity, alcohols

1. Introduction

Functional porous materials are widely applied in industrial fields such as catalysis [1, 2], gas adsorption [3-5] and separations [6, 7]. Understanding and quantifying both the pore structure characteristics and solid-fluid interactions inherent to such materials is critical for the regulation and optimization of chemical processes, and the rational design of new systems. However, detailed characterisation efforts are often hampered by the optically opaque nature of such materials. Nuclear magnetic resonance (NMR) is a non-invasive and chemically selective technique for characterizing porous materials [8-12]. Traditional NMR spectroscopy approaches provide structural information via chemical shift analysis, and are regularly applied to inform the solid state structures of porous materials, including oxides [13, 14], zeolites [15, 16], and porous coordination frameworks and polymers (such as metal-organic- and covalent-organic frameworks) [17-19]. However, for liquids confined within the pore structures of such materials, chemical shift resolution is usually significantly limited by line-broadening effects (especially for standard ^{1}H NMR spectra, which typically exhibit narrow chemical shift ranges), which occur due to local magnetic field distortions caused by magnetic susceptibility differences at the solid-liquid interface [20, 21]. Dynamic NMR measurements are comparatively unaffected by this problem, and instead provide information on the molecular translational and rotational motion of confined species by assessing the decay rates of NMR signals over time [22], with typical means including pulsed field gradient (PFG) NMR diffusion [23] and NMR relaxation time measurements [24]. PFG NMR diffusion measurements are employed to investigate the mass transport of fluids in porous media [25-27], and to quantify the tortuosity of the attendant pore networks [28-32]. NMR relaxation measurements quantify the longitudinal (T_1) and transverse (T_2) relaxation time constants associated with confined fluids; these time constants are directly related to molecular dynamics and can provide valuable information on pore structure characteristics [33-36] and solid-liquid interactions [37-40], especially when screening adsorption processes in sorbents and in catalytically active systems [41-43].

Two-dimensional (2D) $T_1 - T_2$ relaxation time correlation measurements are now employed widely to provide comprehensive information on nuclear spin relaxation processes in porous materials [44-51]. Such measurements provide near-simultaneous information on the T_1 and T_2 relaxation characteristics of confined fluids [52], and further provide facile access to the dimensionless ratio of relaxation time constants (T_1/T_2), which has received particular attention as a non-invasive probe of the relative surface affinities of confined fluids [48-51]. Weber *et al*. [53] were the first to compare the surface interaction strengths of reagents and solvents within liquid phase catalytical systems based on the acquisition of T_1/T_2 values from 2D correlation measurement, and demonstrated the ability of such

data to differentiate multiple proton relaxation environments associated with different adsorbates simultaneously. Robinson *et al*. [54] observed that polar-protic adsorbates (short chain alcohols and carboxylic acids) confined to mesoporous silica with a single pore size showed two distinct relaxation populations within 2D $T_1 - T_2$ correlations when using short echo times and low-magnetic-field strengths, which were significantly different from a single correlation peak of confined water [48, 55]. These correlation peaks were assigned to different proton environments associated with adsorbate alkyl ($C_x{}^1H_y$) and hydroxyl groups ($-O^1H$), with these assignments supported by the relative integrated intensities of the observed peaks [54]; such observations have since been extended to C_3 hydrocarbons within mesoporous gamma alumina [56], and are consistent with the work of Ward-Williams *et al*. on the fast field cycling relaxation dynamics of confined methanol [57-59].

Due to the decreased molecular mobility at the solid-liquid interface, together with dipolar coupling interactions between adsorbates and spins embedded within the pore surface, the relaxation rates (T_i^{-1}, $i \in \{1, 2\}$) of liquids confined within porous materials will be enhanced compared to the associated unrestricted bulk liquid [60]. For typical systems exhibiting a low concentration of pore surface-bound paramagnetic species, the enhanced relaxation rates of confined liquids are linearly related to the surface-to-volume ratio of the porous material [61]. The scaling factor that quantifies the ability of the solid-liquid interface to enhance relaxation is termed the surface relaxivity [62], and is usually calibrated by independent measurements of pore characteristics and enhanced relaxation rates [63]. While surface relaxivity quantification provides a potential approach to assess the structural characteristics of liquid-saturated porous materials based on the measurement of relaxation responses alone [64-66], a problem of significant concern is that even in materials with a single, well-defined pore size, confined probe liquids with multiple proton environments may exhibit multiple significantly different relaxation rates [54], corresponding to a variety of surface relaxivities. Molecules exhibiting multiple proton environments associated with different functional groups are common in organic and synthetic chemistry, and include solvents and reagents (e.g. methanol and 2-propanol) used for the functionalization of porous materials [67], and in catalytic reactions [53, 68]. Notably, the relationship between the enhanced relaxation rates of these different functional groups and the surface-to-volume ratio of confining pore structures is still unclear, which hinders extensive exploration of the pore structure characteristics and interfacial phenomenon of fluid-saturated functional porous materials using NMR. As such, in this study we systematically evaluate the surface relaxation characteristics of a series of ten common solvents confined to four commercial mesoporous silicas with nominal (meso)pore diameters between 6 nm and 50 nm. We demonstrate the clear identification of functional group specific relaxation characteristics associated with the different proton-bearing chemical moieties

(alkyl and hydroxyl groups) of the polar protic adsorbates assessed, and for the first time quantify the different surface relaxivities of these groups.

2. Surface Relaxation Theory

For liquid-saturated porous media, the observed relaxation rates $T_{i,\mathrm{obs}}^{-1}$ (where $i = 1$ for longitudinal and $i = 2$ for transverse relaxation) of confined spin-bearing fluids may be expressed as a linear combination of bulk, surface and diffusion terms [64, 69]:

$$\frac{1}{T_{1,\mathrm{obs}}} \approx \underbrace{\frac{1}{T_{1,\mathrm{bulk}}}}_{\text{bulk}} + \underbrace{\rho_1 \frac{S}{V}}_{\text{surface}}, \tag{1}$$

$$\frac{1}{T_{2,\mathrm{obs}}} \approx \underbrace{\frac{1}{T_{2,\mathrm{bulk}}}}_{\text{bulk}} + \underbrace{\rho_2 \frac{S}{V}}_{\text{surface}} + \underbrace{a t_{\mathrm{e}}^{(k-1)}}_{\text{diffusion}}. \tag{2}$$

Here, $T_{i,\mathrm{obs}}$ are the observed relaxation time constants of the confined liquid, $T_{i,\mathrm{bulk}}$ are the time constants of the unrestricted bulk liquid, and S/V is the surface-to-volume ratio of the confining pore structure. The terms ρ_i are the (spatially averaged) surface relaxivities of the solid-liquid interface; formally, these terms quantify the enhanced rates of nuclear spin relaxation which occur within the adsorbed surface layer of fluid-filled pore structures, and may be expanded as $\rho_i = \lambda/T_{i,\mathrm{surf}}$, where λ is the thickness of the adsorbed surface layer across which surface enhanced relaxation rates occur, and $T_{i,\mathrm{surf}}$ are the relaxation time constants of adsorbates within that layer [56]. Collectively, this surface term therefore provides sensitivity to both surface and interfacial chemistry (via ρ_i) and material pore structure (via S/V). The diffusion term provides a perturbation to observed transverse relaxation ($T_{2,\mathrm{obs}}$) as a result of spin diffusion through effective magnetic field gradients within the confining pore structure, which originate from magnetic susceptibility contrast at the solid/liquid interface [70] (T_1 relaxation is unaffected by such susceptibility contract effects [71]), while the term t_{e} is the experimental echo time within the NMR pulse sequence. For non-viscous liquids confined to mesoporous media (with pore diameters between 2 and 50 nm), the parameters k and a are well-defined [69], with $k = 1$ and $a = \gamma^2 g^2 \ell_s^4/(120D)$. Here γ is the gyromagnetic ratio of the ^{1}H nucleus, g is the average magnetic field gradient across the pore structure of interest, ℓ_s is the length scale of the confining pore structure, and D is the self-diffusion coefficient of the confined liquid. As $g \sim \Delta\chi B_0$, i.e. such gradients scale in magnitude with both susceptibility contrast $\Delta\chi$ and applied magnetic field strength B_0, the influence of this diffusion term on observed transverse relaxation rates may be mitigated by the application of comparably low magnetic field strength NMR equipment, as was performed in this study (see Section 3.2). As such, Equations (1) and (2) may be rewritten in terms of

enhanced relaxation rates ($T_{i,\mathrm{E}}^{-1}$), such that

$$\frac{1}{T_{i,\mathrm{E}}} = \frac{1}{T_{i,\mathrm{obs}}} - \frac{1}{T_{i,\mathrm{bulk}}} = \rho_i \frac{S}{V}, \tag{3}$$

where surface relaxivity values (ρ_i) can be evaluated using a linear fit between $T_{i,\mathrm{E}}^{-1}$ and measured pore surface-to-volume ratio (S/V). It should be noted that a precondition of Equation (3) is the fast diffusion assumption of surface relaxation [61]. For the fast diffusion (also termed surface-limited relaxation [72]), the diffusion rate through the pores is significantly more rapid than the rates of surface relaxation. Conversely, slow diffusion (also termed diffusion-limited relaxation [72]) refers to situations where surface relaxation rates are significantly more rapid than diffusion across the pore [73]. The parameter κ_i separates fast diffusion ($\kappa_i \ll 1$) and slow diffusion ($\kappa_i \gg 1$) according to [61, 74]:

$$\kappa_i = \frac{\rho_i}{2D} \cdot \frac{\alpha V}{S}, \tag{4}$$

where α is geometric factor that takes values $\alpha = 1$, 2 and 3 for slit, cylindrical and spherical pores, respectively. When the fast diffusion assumption is not satisfied, spatially averaged surface relaxivities can be calculated using a more general form that applies to the intermediate regime between fast and slow diffusion [74].

3. Methods

3.1. Materials and Sample Preparation

CARiACT Q-series mesoporous silica gel materials (Q6, Q15, Q30, and Q50) comprising spherical particles of nominal diameter 1.7−4.0 mm were supplied by Fuji Silysia Chemical Ltd. (Japan); the number in the Q-series silica label indicates the reported average pore diameter in units of nm. Cyclohexane (Ajax Finechem, >99.0%), acetone (EMSURE, >99.8%), methanol (ChemSupply Australia, >99.9%), ethanol (ChemSupply Australia, >99.5%), 1-propanol (ChemSupply Australia, >99.8%), 1-butanol (ChemSupply Australia, >99.0%), 2-propanol (ChemSupply Australia, >99.5%), 2-butanol (ChemSupply Australia, >99.0%), ethylene glycol (ChemSupply Australia, >99.9%) were used as received. Deionized water was provided on site.

To homogenize the surface hydroxyl environments of the Q-series silicas, each material was first refluxed in deionized water for 12 h, then dried in air at 110 ℃ for 24 h. For dried silicas, nitrogen isotherm analysis was conducted at 77 K using a Micromeritics ASAP 2020 Adsorption Analyser. The resulting Barrett-Joyner-Halenda (BJH) desorption pore size distributions and pore volumes, together with Brunauer-Emmett-Teller (BET) adsorption specific surface areas, are provided in Supporting Information Note 1. Furthermore, the surface hydroxyl density of each silica material was measured using the liquid phase deuterium exchange technique proposed by Penrose *et al*. [75] (see Supporting Information Note 2).

For NMR relaxation analysis, dried silicas were generally soaked in excess liquid for at least 48 h at room temperature (25±1 ℃). For the more viscous probe liquids explored (ethylene glycol, 1-butanol and 2-butanol) an additional heating process was applied (50 ℃ for 5 h) to ensure that the solvents could adequately penetrate the silica pore network. The silicas were then separated from the excess liquid and rolled on a pre-soaked filter paper to remove interparticle liquid. They were then quickly transferred to sealed 7 ml glass vials to minimize liquid evaporation; filling factors [76] for each saturated silica sample were found to be ≥0.94 and were assessed gravimetrically. Each sample consisted of approximately 6.5 g of imbibed silica (corresponding to ~240 particles), facilitating well-averaged measurements of the surface-adsorbate interactions present between each imbibed liquid and the pore surfaces present throughout the mesoporous silicas investigated. A total of 10 separate bulk liquids (~ 5 ml) were also individually sealed in 7 ml glass vials.

3.2. NMR Hardware and Relaxation Measurements

NMR relaxation measurements were performed using a benchtop Oxford Instruments GeoSpec

NMR spectrometer equipped with a 0.3 T parallel plate magnet array (providing a ^{1}H frequency of ν_0=12.7 MHz at the default magnet temperature of T_d = 30 °C) and 53 mm Q-sense probe. All sample vials were placed in the centre of the magnet bore, as confirmed via the acquisition of a one-dimensional profile image before analysis.

$T_1 - T_2$ relaxation correlation data were acquired using the 2D radio frequency (RF) pulse sequence shown in Figure 1 [52]. Here, a 180° RF pulse first rotates the sample magnetization from the z-axis (aligned parallel to the static magnetic field) to the −z-axis, initiating longitudinal relaxation (along the +z direction) towards thermal equilibrium within the variable recovery time τ, which encodes T_1. A 90° RF pulse then rotates the sample magnetization into the x-y plane, and is followed by a train of n 180° RF refocusing pulses separated by an echo time t_e, generating n spin echoes of magnitude $S(\tau, nt_e)$ (black data point in Figure 1), which decay in magnitude according to T_2. The pulse sequence was cycled with m different τ recovery times, forming a ($m \times n$) data surface which encodes both T_1 and T_2 relaxation information. For imbibed silica samples, T_1 was encoded using m = 64 logarithmically spaced τ recovery times from 1 ms to 6 s. In general, T_2 was encoded by recording magnitude of n = 18000 echoes separated by an echo time of t_e = 100 μs, although for the cyclohexane-saturated silica samples n = 48000 echoes was employed to capture the full T_2 decay of the system. For bulk liquid samples, T_1 was encoded by using m = 32 logarithmically spaced τ recovery times from 1 ms to 25 s. In general, T_2 was encoded by recording magnitude of n = 48000 echoes with an echo time t_e = 300 μs; the bulk acetone sample used n = 62000 echoes. All measurements employed 4 repeat scans to provide signal averaging, and the recycle delay between each repeat scan was 15 s (≫5 × T_1), resulting in an acquisition time of approximately 80 minutes.

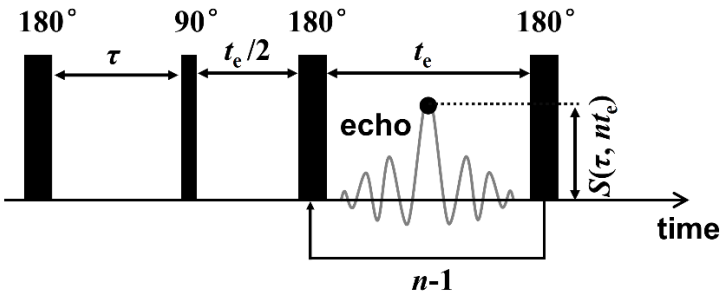

Figure 1. Schematic diagram of the $T_1 - T_2$ ^{1}H radio frequency (RF) pulse sequence applied in this work. Thick and thin bars represent 180 and 90° RF pulses, respectively, while the black data point represents the measured spin echo magnitudes $S(\tau, nt_e)$. The variables τ, n and t_e are defined in the main text.

3.3. Data Processing

The acquired data surface resulting from $T_1 - T_2$ relaxation correlation measurements is described by a 2D Fredholm integral equation [77]:

$$\frac{S(\tau,nt_e)}{S(\infty,0)} = \iint K_{12}(\tau, T_1, nt_e, T_2)F(T_1, T_2)d\log_{10}(T_1)d\log_{10}(T_2) + \varepsilon(\tau, nt_e), \quad (5)$$

where $S(\tau, nt_e)/S(\infty, 0)$ is the normalized spin echo magnitude, and $\varepsilon(\tau, nt_e)$ is the experimental noise; $F(T_1, T_2)$ is the targeted distribution of T_1 and T_2 relaxation time constants, while the kernel function $K_{12}(\tau, T_1, nt_e, T_2)$ describes the expected form of T_1 and T_2 relaxation across the experimental pulse sequence employed:

$$K_{12}(\tau, T_1, nt_e, T_2) = \left\{1 - 2\exp\left(\frac{-\tau}{T_1}\right)\right\}\exp\left(\frac{-nt_e}{T_2}\right). \quad (6)$$

According to Equations (5) and (6), $F(T_1, T_2)$ can be acquired by a numerical inversion (often termed a Laplace inversion or inverse Laplace transform) based on the acquired 2D relaxation data. In the presence of experimental noise, a stable distribution of relaxation time constants was achieved by using Tikhonov regularization [78], with the degree of smoothing determined by the Generalised Cross Validation method [79]. The resulting $T_1 - T_2$ relaxation correlation distributions were limited to (200 × 200) values with output ranges (10^{-4} to 10^{1}) s in each dimension. The above numerical inversions were performed using a fast Laplace inversion algorithm written by Mitchell *et al*. [80] in MATLAB (MathWorks Inc.).

4. Results and Discussion

4.1. Relaxation Correlation Measurements of Confined Adsorbates

Figure 2 demonstrates $T_1 - T_2$ correlation data from cyclohexane and acetone (considered here as prototypical apolar aprotic and polar aprotic adsorbates, respectively) confined within the mesoporous silicas Q6, Q15, Q30 and Q50. As all interparticle liquid was removed prior to NMR analysis (see Section 3.1), the observed relaxation phenomena must characterise confined liquids within the silica pore structures. A single, narrow relaxation time distribution is observed in each case, which following the simple surface relaxation theory described in Section 2 indicates that the materials explored here do not demonstrate a hierarchical pore structure; this observation is supported by pore size distributions detailed in Supporting Information Note 1. Importantly, as relaxation correlation peak shapes are highly sensitive to experimental noise [77], we focus here only on the modal relaxation times of such peaks (termed $\langle T_1 \rangle$ and $\langle T_2 \rangle$), together with their modal ratio $\langle T_1/T_2 \rangle$, which is quantified at the maximum value of each correlation peak. As a useful example, the observed $\langle T_1/T_2 \rangle$ ratios for Q15 are indicated by red dashed diagonal lines in Figure 2. D'Agostino *et al*. [48] and Robinson *et al*. [49] found that the $\langle T_1/T_2 \rangle$ ratio can be related directly to the adsorption energy of liquids within heterogeneous catalyst supports, and this ratio is now generally considered a rapid and non-invasive probe of the surface affinities of liquids absorbed in porous materials [42, 51]. As shown in Figure 2, the $\langle T_1/T_2 \rangle$ ratio of cyclohexane ($\langle T_1/T_2 \rangle \approx 1.12$) in Q15 is lower than that of acetone within the same material ($\langle T_1/T_2 \rangle \approx 1.44$). This result indicates that the surface affinities of these adsorbates can be ranked as cyclohexane < acetone, which is consistent with the order of the relative polarity values of these molecules [81].

Figure 3(a-h) shows $T_1 - T_2$ correlation data acquired from confined polar protic adsorbates in Q6, Q15, Q30 and Q50, including deionized water, four primary alcohols (methanol, ethanol, 1-propanol, and 1-butanol), two secondary alcohols (2-propanol and 2-butanol), and one polyol (ethylene glycol). The $\langle T_1/T_2 \rangle$ ratio of water ($\langle T_1/T_2 \rangle \approx 7.15$) in Q15 is larger than that of both acetone and cyclohexane, likely reflecting the comparably stronger interaction between adsorbed water and the polar surfaces of the silica pores. For confined alcohols, two distinct correlation peaks are clearly apparent in each data set, which are characterised by different $\langle T_1 \rangle$ and $\langle T_2 \rangle$ values (and in some cases $\langle T_1/T_2 \rangle$ ratios; detailed relaxation time values are provided in Supporting Information Note 3). Given that no hierarchical structure is present in these materials, this observation is attributed to the existence of multiple different proton relaxation environments within each polar protic adsorbate, consistent with our recent work using both Q15 silica [54] and mesoporous gamma alumina [56]. To further verify these correlation peak assignments, Figure 3(i) details the observed alkyl/hydroxyl ratio of each

adsorbate calculated from the integrals of the two correlation peaks in our Q15 data; a strong correlation between observed and expected alkyl/hydroxyl ratios is evident. The clear observation of hydroxyl group relaxation across the entire series of alcohols assessed is attributed to the low magnetic field strength and short echo time employed here [56, 58, 82]. Furthermore, in extension to our previous research [54], these data demonstrate – to the best of our knowledge – the first reported observation of functional group resolved nuclear spin relaxation within polyol (ethylene glycol) saturated mesoporous silicas, demonstrating and extending the unique ability of low-field NMR relaxation to non-invasively observe and identify functional group specific relaxation phenomena associated with a wide range of organic solvents and reagents confined to porous materials.

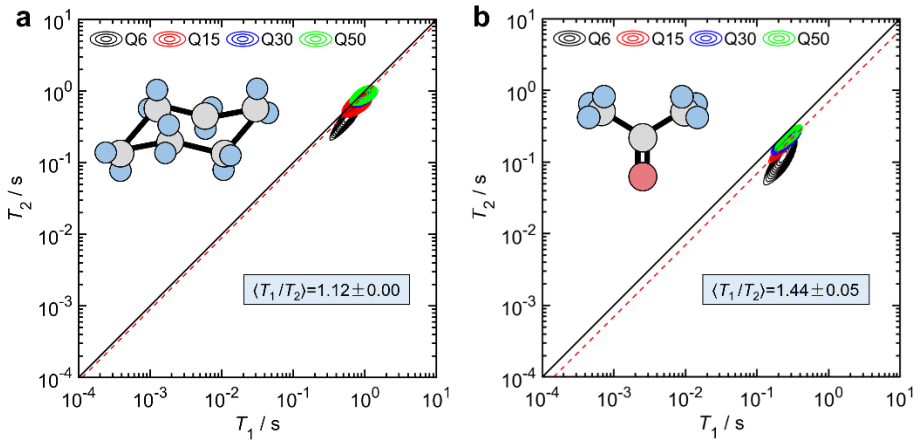

Figure 2. ^{1}H T_1–T_2 correlation plots of confined (a) cyclohexane and (b) acetone in Q6, Q15, Q30 and Q50 mesoporous silicas. Solid diagonal lines indicate the relaxation time ratio T_1/T_2 = 1, while red dashed diagonal lines indicate the observed modal relaxation time ratio $\langle T_1/T_2 \rangle$ of each correlation peak in Q15 as example; reported uncertainties in $\langle T_1/T_2 \rangle$ correspond with the observed standard deviation in peak maximum across three repeat measurements on the same sample. The molecular structure of each adsorbate is indicated in each case, where C, O, and aprotic H atoms are colored gray, red, and blue, respectively.

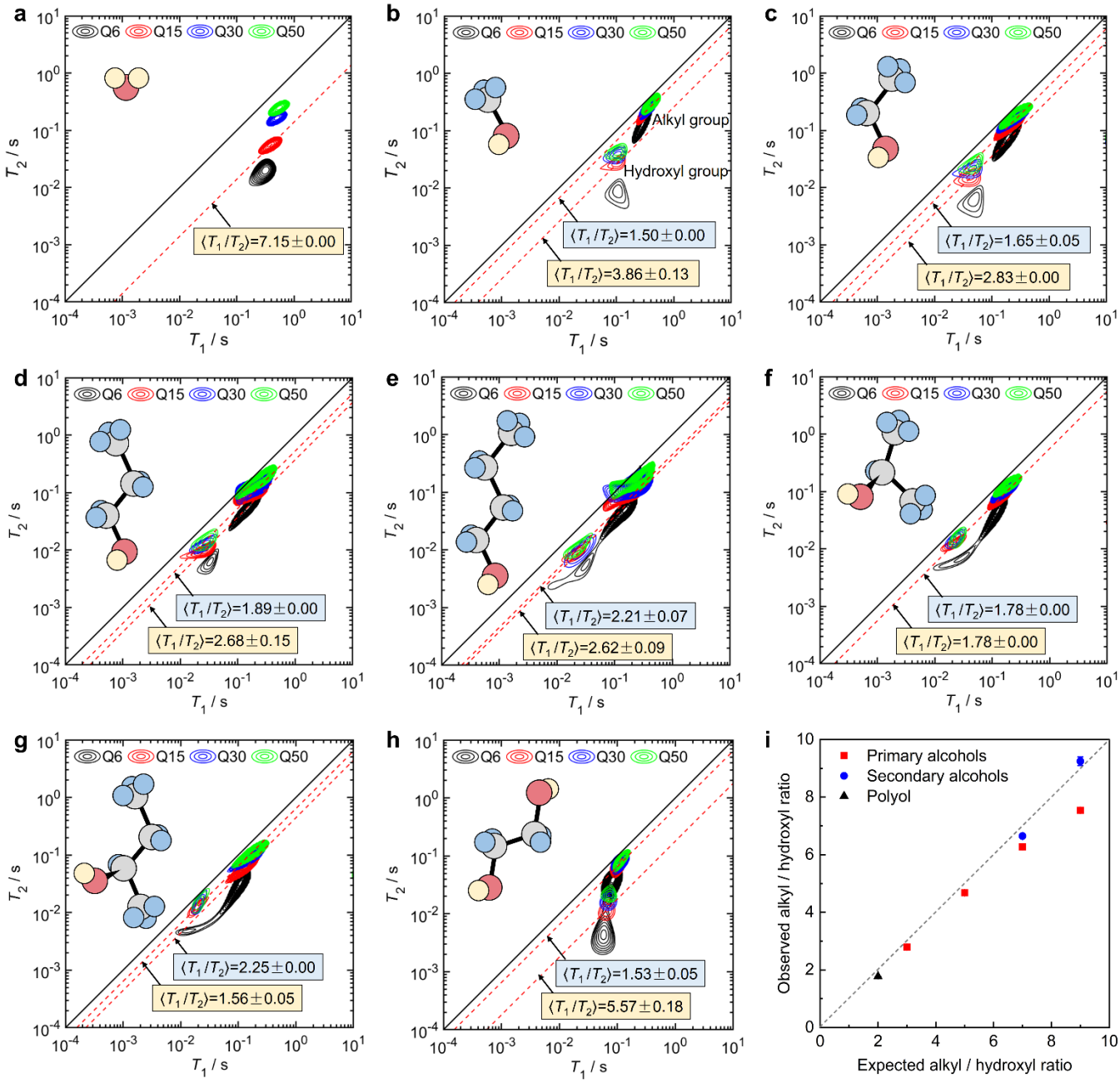

Figure 3. ^{1}H T_1–T_2 correlation plots of confined (a) deionized water, (b-e) primary alcohols [(b) methanol, (c) ethanol, (d) 1-propanol, and (e) 1-butanol], (f-g) secondary alcohols [(f) 2-propanol and (g) 2-butanol], and (h) ethylene glycol in Q6, Q15, Q30 and Q50 mesoporous silicas. Solid diagonal lines indicate the relaxation time ratio T_1/T_2 = 1, while the red dashed diagonal lines indicate the observed modal relaxation time ratio $\langle T_1/T_2 \rangle$ of each correlation peak in Q15 as an example; reported uncertainties in $\langle T_1/T_2 \rangle$ correspond with the observed standard deviation in peak maximum across three repeat measurements on the same sample. The molecular structure of each adsorbate is indicated in each case, where C, O, aprotic H and protic H are colored gray, red, blue and yellow, respectively. Correlation peaks at long and short T_2 are assigned to aprotic alkyl groups ($C_x{}^1H_y$) and protic hydroxyl groups ($-O^1H$), respectively. (i) Observed alkyl/hydroxyl ratio of each adsorbate (acquired from the integrated ratio of the two observed correlation peaks) in Q15 only as a function of expected alkyl/hydroxyl ratio (acquired from the number ratio of aprotic and protic H atoms). The dashed line in (i) denotes parity between the two axes; error bars are generally smaller than the depicted data points and indicate the observed standard deviation from three repeat measurements on the same sample.

Figure 4(a) provides a summary of the modal relaxation time ratios $\langle T_1/T_2 \rangle$ of both hydroxyl and alkyl ^{1}H groups of alcohols imbibed within Q15. For both primary and secondary alcohols, the $\langle T_1/T_2 \rangle$ ratio of the hydroxyl group decreases as a function of increasing carbon chain length, while the alkyl group increases, demonstrating the opposite trend. The metric $\Delta\langle T_1/T_2 \rangle = \langle T_1/T_2 \rangle_{\text{hydroxyl}} - \langle T_1/T_2 \rangle_{\text{alkyl}}$ (where subscripts define either the hydroxyl or alkyl ratio) provides a simple approach to quantify the difference in $\langle T_1/T_2 \rangle$ ratio between functional groups, and in previous work has been observed to correlate strongly with adsorbate acidity [54]. Specifically, a higher degree of adsorbate acidity (indicated by low pK_a values) leads to facile surface-adsorbate proton exchange between surface and adsorbate hydroxyl groups; such dynamics lead to the observed hydroxyl relaxation characterisatics of our adsorbates exhibiting solid-like properties with simultaneously longer T_1 times and shorter T_2 times (corresponding to large $\Delta\langle T_1/T_2 \rangle$), while adsorbate alkyl groups do not undergo such proton exchange. As shown in Figure 4(b), ethylene glycol also conforms to the above trend, which is demonstrated to hold across the range of mesopore sizes examined here. The effect of adsorbate acidity on $\Delta\langle T_1/T_2 \rangle$ is more obvious for alcohols confined in small pore-size silicas; this observation is attributed to the very short hydroxyl T_2 times observed for these materials, which result in correspondingly large $\langle T_1/T_2 \rangle_{\text{hydroxyl}}$ values.

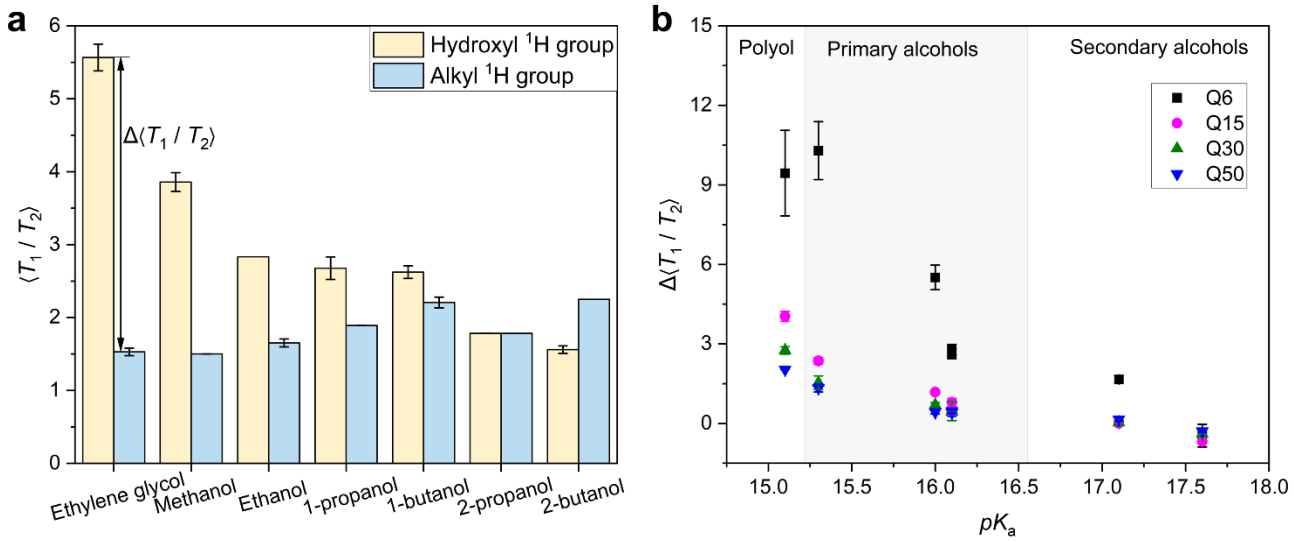

Figure 4. (a) Summary of the modal relaxation time ratios $\langle T_1/T_2 \rangle$ of both hydroxyl and alkyl ^{1}H groups of imbibed alcohols in Q15. (b) Correlation between the difference in modal relaxation time ratios of hydroxyl and alkyl groups $\Delta\langle T_1/T_2 \rangle$ and adsorbate pK_a.

4.2. Dependence of Enhanced Relaxation on Pore Surface-to-Volume Ratio

In this section, we further explore the dependence of the enhanced relaxation rates of the above series of confined adsorbates on silica pore surface-to-volume ratio (S/V, as measured by gas sorption; see Section 3.1). We again use the modal relaxation time constants of the confined liquids, as well as values from equivalent measurements of unrestricted bulk liquids (see Supporting Information Note 3), to calculate enhanced relaxation rates ($\langle T_{i,\mathrm{E}} \rangle^{-1}$).

Figure 5 shows the dependence of longitudinal and transverse enhanced relaxation rates of confined cyclohexane and acetone on S/V. For cyclohexane, both the longitudinal and transverse relaxation data of all materials scale linearly with S/V. For acetone, data acquired from Q15, Q30 and Q30 again scales linearly within S/V, while the calculated enhanced relaxation rates of Q6 appear anomalous. In each case, the resulting linear fits show unexpectedly large (non-zero) y-intercepts, which are inconsistent with Equation (3). We rationalize this observation by considering the simple relaxation rate contribution theory proposed by Faux *et al*. [83]. Considering the typical biphasic fast exchange model for a liquid-saturated pore, adsorbates may be found either within the adsorbed surface layer near the pore walls, or within a bulk-like region (the "pore bulk") towards the centre of the pore. While the overall observed relaxation rates are a weighted average of the rates within these two regions, a complete description must also recognise that the inherent relaxation rates of each region are influenced by the existence of the other (specifically, via intermolecular dipolar coupling interactions, which facilitate the microscopic magnetic fluctuations responsible for nuclear spin relaxation [82]). The relaxation rates of the pore bulk (now termed $T_{i,\mathrm{pb}}^{-1}$) therefore comprise a linear combination of contributions from both bulk-bulk interactions ($T_{i,\mathrm{bb}}^{-1}$) and interactions between the pore bulk and the adsorbed surface layer ($T_{i,\mathrm{bl}}^{-1}$), such that $T_{i,\mathrm{pb}}^{-1} = T_{i,\mathrm{bb}}^{-1} + T_{i,\mathrm{bl}}^{-1}$. This expression is different to that governing relaxation within entirely unrestricted bulk liquid, which will contain no contribution from $T_{i,\mathrm{bl}}^{-1}$, such that $T_{i,\mathrm{bulk}}^{-1} \equiv T_{i,\mathrm{bb}}^{-1} < T_{i,\mathrm{pb}}^{-1}$, resulting in an underestimation of pore bulk relaxation rates in our measurements and hence non-zero y-intercepts when fitting our data using Equation (3). Calculated $T_{i,\mathrm{pb}}$ values are provided in Supporting Information Note 4; however, given the above observation does not significantly influence the linear correlations observed in our results, in the remainder of this work we focus exclusively on the gradient of our linear fits, rather than further discussion of the resulting intercepts.

Figure 6(a-b) shows the dependence of longitudinal enhanced relaxation rates for both the alkyl and hydroxyl groups of confined polar protic adsorbates on S/V. These data demonstrate a clear linear relationship for all adsorbates up to $S/V \sim 200$ μm^{-1}, as predicted by Equation (3), while high S/V data acquired from Q6 again lies outside of the predicted trend. Conversely, Figure 6(c-d) shows an

excellent linear relationship between the transverse enhanced relaxation rates and S/V for both the alkyl hydroxyl groups of confined species across all four mesoporous silicas investigated (up to $S/V \sim 600$ μm^{-1}). While fully elucidating upon the origin of the (partially) anomalous relaxation behavior shown by Q6 is the subject of ongoing investigations, we suggest the non-conformity of these data may arise from subtle differences in pore surface chemistry between different silica materials, which will be accentuated by the very large S/V values inherent to Q6. We note that overall measured Q6 surface hydroxyl density values are equivalent to that of Q15 ($\alpha_{OH} \sim 3.7$ nm^{-2}; see tabulated data in Supporting Information Note 2); however, such data does not take into account the potential for different types of surface hydroxyl groups (isolated [Si-O-H], hydrogen bonded [Si-O-H···O(H)-Si] or geminal [Si-$(OH)_2$]) or their microscopic distribution across the pore surface, nor do these data inform on the surface accessibility of very low levels of any paramagnetic contaminants present.

Importantly, under the fast diffusion assumption of surface relaxation, the gradient of our linear fits in Figures 5 and 6 may be directly interpreted as the surface relaxivities (ρ_i) of each spin-bearing group at the attendant solid/fluid interface. The validity of applying this assumption was evaluated using Equations (4) (verification details are provided in Supporting Information Note 5); our calculations resulted in a maximum value of $\kappa_i = 0.026 \ll 1$, confirming that all the experimental systems assessed here satisfy the requirement for fast diffusion. The resulting surface relaxivity values are detailed in Table 1 (further data is provided in Supporting Information Note 4). We note from these data that for both the alkyl and hydroxyl groups of our adsorbate series, fitted ρ_2 values are found to be universally larger than the resulting ρ_1 values; such results are consistent with previous investigations on the surface relaxivities of confined water in porous silica [51, 84], and demonstrate quantitively that solid-liquid interactions within our saturated mesoporous silicas enhance transverse nuclear spin relaxation rates to a greater degree than longitudinal relaxation rates. However, Supporting Information Note 4 further details the uncertainties obtained from our linear fitting process; for multiple adsorbates, uncertainties in values of the longitudinal surface relaxaivity ρ_1 are unacceptably large (>100 % in some cases), precluding any detailed evaluation of these data. As such, in the remainder of this work we focus on interpretation of the transverse surface relaxaivity values alone.

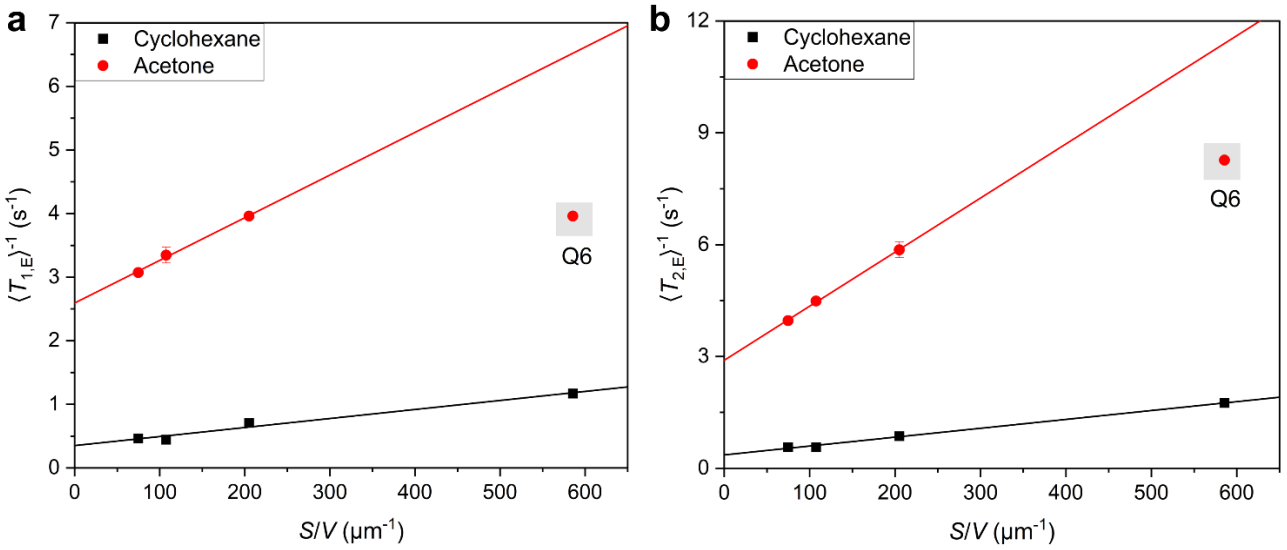

Figure 5. Dependence of the (a) longitudinal enhanced relaxation rates ($\langle T_{1,E}\rangle^{-1}$), and (b) transverse enhanced relaxation rates ($\langle T_{2,E}\rangle^{-1}$) of confined cyclohexane and acetone on the pore surface-to-volume ratio (S/V) of mesoporous silicas. Lines indicate a linear fit to the data (detailed fitting results are provided in Supporting Information Note 4). For cyclohexane, this fitting is based on the complete Q6, Q15, Q30, and Q50 data set. For acetone, fitting is based on only Q15, Q30, and Q50 data.

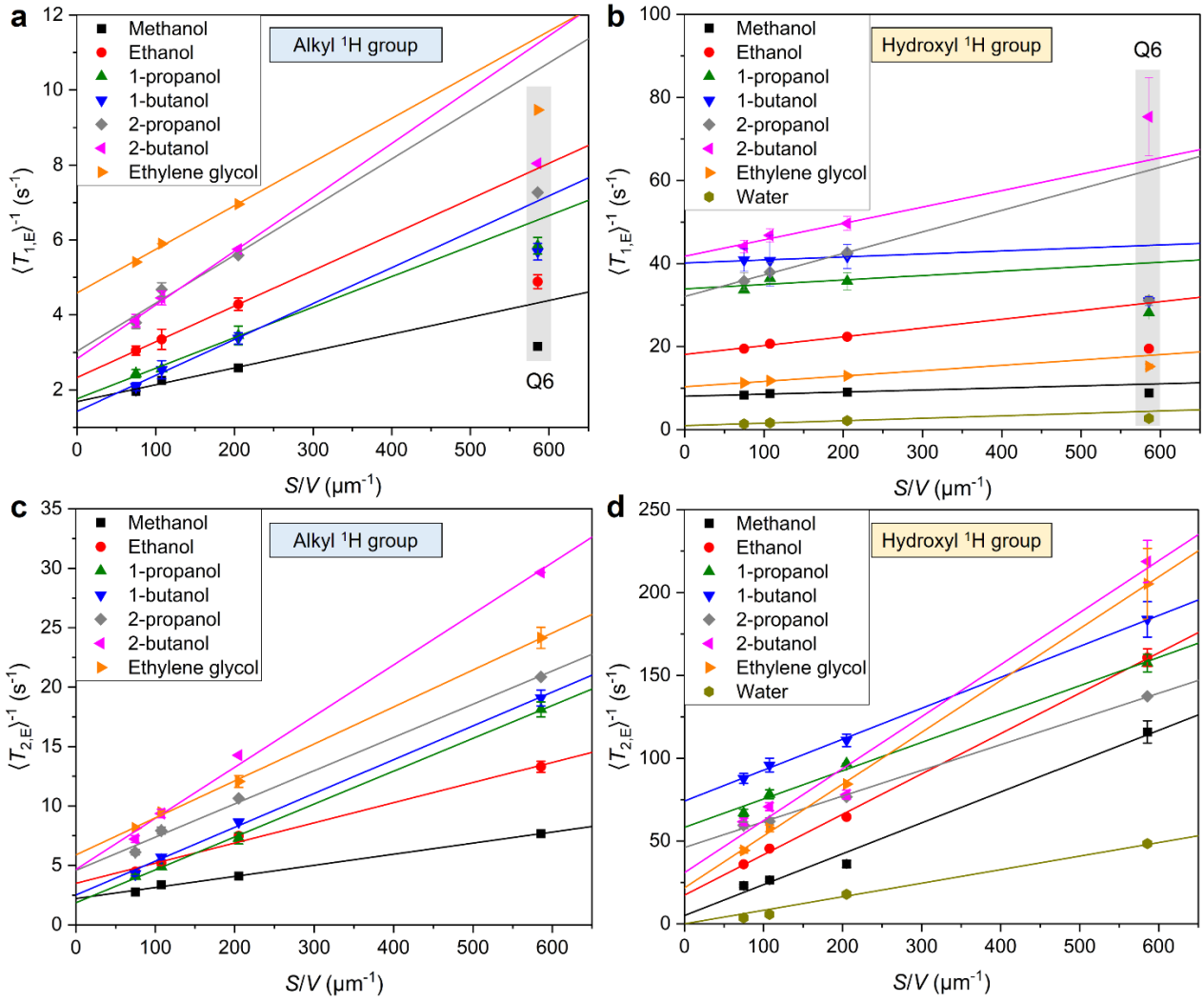

Figure 6. Dependence of the longitudinal enhanced relaxation rates ($\langle T_{1,E}\rangle^{-1}$) for (a) alkyl groups, and (b) hydroxyl groups in confined polar protic adsorbates, together with transverse enhanced relaxation rates ($\langle T_{2,E}\rangle^{-1}$) for (c) alkyl groups, and (d) hydroxyl groups of confined polar protic adsorbates on the pore surface-to-volume ratio (S/V) of mesoporous silicas. Lines indicate a linear fit to the data (detailed fitting results are provided in Supporting Information Note 4). For longitudinal relaxation each fit is based on only Q15, Q30, and Q50 data. For transverse relaxation each fit is based on the complete Q6, Q15, Q30, and Q50 data set.

Table 1. Longitudinal and transverse surface relaxivities from the linear fits detailed in Figures 5 and 6.

Adsorbate	Alkyl group		Hydroxyl group	
	ρ_1 (μm / s)	ρ_2 (μm / s)	ρ_1 (μm / s)	ρ_2 (μm / s)
Cyclohexane	0.0014	0.0024	-	-
Acetone	0.0067*	0.0145*	-	-
Water	-	-	0.0059*	0.0818
Methanol	0.0045*	0.0093	0.0050*	0.1864
Ethanol	0.0095*	0.0170	0.0212*	0.2439
1-propanol	0.0082*	0.0277	0.0108*	0.1712
1-butanol	0.0096*	0.0285	0.0072*	0.1869
2-propanol	0.0128*	0.0280	0.0519*	0.1553
2-butanol	0.0144*	0.0430	0.0395*	0.3140
Ethylene glycol	0.0116*	0.0311	0.0129*	0.3130

* Fitting based on Q15, Q30, and Q50 data only

4.3. Transverse Surface Relaxivity and Molecular Structure

Given the strong dependence of functional group resolved transverse enhanced relaxation rates on silica pore *S/V*, it is of interest to explore how adsorbate structure correlates with transverse surface relaxivity more closely. Fitted ρ_2 values are summarised in Figure 7(a); the ρ_2 of water is 0.0818 ± 0.0122 μm/s, which is close to the ranges reported previously by D'Orazio *et al*. (0.109-0.214 μm/s for porous silica glass [84]) and Krzyżak *et al*. (0.12-0.17 μm/s and 0.18-0.20 μm/s for mesoporous silica materials MCM-41 and SBA-15, respectively [51]). Notably, for confined alcohols, the ρ_2 value of each hydroxyl group is consistently 5-20 times that of the corresponding alkyl group. We rationalize this difference by recalling that hydrogen bond mediated adsorption interactions will dominate the alcohol/silica interface [54]. Such interactions lead to short dipolar coupling distances r between surface and adsorbate hydroxyl groups. As surface relaxation rates generally scale with such distances as $T_{2,\mathrm{surf}}^{-1} \propto r^{-3}$ [85], this adsorption mode will increase hydroxyl surface relaxation rates (leading to large associated surface relaxivity values $\rho_2 = \lambda/T_{2,\mathrm{surf}}$) relative to those of the corresponding alkyl group; the resulting hydroxyl ρ_2 values will also be further enhanced by the surface-adsorbate proton exchange interactions discussed in Section 4.1. It is of further interest to consider that values of the length scale λ (which defines the thickness of the adsorbed surface layer across which surface enhanced relaxation dominates) are therefore expected to be different when considering alkyl or hydroxyl group relaxivity. For hydroxyl groups, we propose that this length scale will be on the order of surface-adsorbate hydrogen bonding distances ($\lambda \sim 3$ Å), while for alkyl groups this may extend one or more molecular layers from the pore surface. We note that these suggestions are in keeping with concept of the distance of closest approach between interacting dipoles within the formal theory of surface relaxation [72].

As illustrated in Figure 7(a), alkyl group ρ_2 values for the four primary alcohols investigated are ranked: methanol (0.0093 ± 0.0016 μm/s) < ethanol (0.0170 ± 0.0046 μm/s) < 1-propanol (0.0277 ± 0.0022 μm/s) < 1-butanol (0.0285 ± 0.0036 μm/s), while alkyl group ρ_2 values for secondary alcohols are ranked: 2-propanol (0.0280 ± 0.0055 μm/s) < 2-butanol (0.0430 ± 0.008 μm/s). These trends track well with the known order of surface affinity within these adsorbates, which increase both with increasing carbon chain length and upon moving from primary to secondary alcohols [49, 54]. In Figure 7(b) we provide a clear illustration of this apparent dependence on molecular structure by evaluating the alky/hydroxyl ratio of each adsorbate. Importantly, this plot demonstrates a strong, linear relationship between transverse surface relaxivity and alcohol structure, providing – to our knowledge – the first evidence of simple, quantitative relationships between surface relaxivity and adsorbate chemistry. Large relative uncertainties in hydroxyl group ρ_2 values unfortunately preclude

the assignment of any significant trends in these data as a function of varying molecular structure.

Finally, due to the obvious distinction between alkyl and hydroxyl groups along the T_2 dimension of the relaxation correlation plots in Figure 3, we further extracted one-dimensional (1D) T_2 decays from our 2D correlation data. Calculations of the corresponding ρ_2 values from these 1D data reveal an almost identical correlation with alkyl/hydroxyl ratio as demonstrated in Figure 7(b) (see Supporting Information Note 6), demonstrating that the acquisition of simple 1D T_2 data may be applied as a rapid means of assessing functional group resolved transverse surface relaxivities.

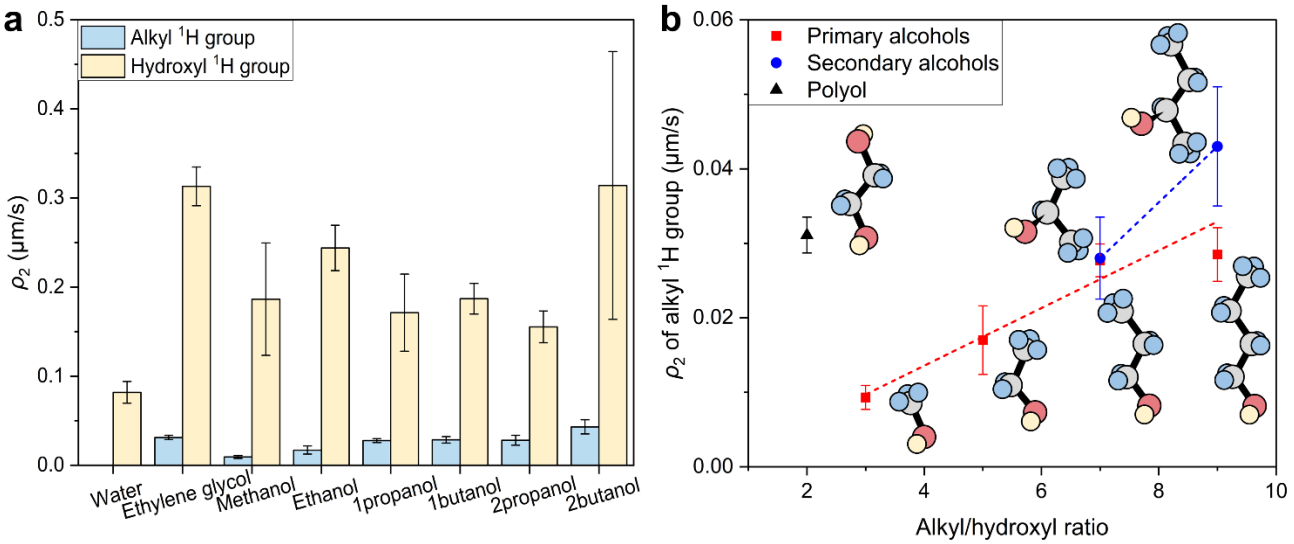

Figure 7. (a) Transverse surface relaxivities (ρ_2) of the alkyl group and hydroxyl group of confined polar protic adsorbates in mesoporous silica. (b) Transverse surface relaxivities of the alkyl group as a function of adsorbate alkyl/hydroxyl ratio (acquired from the number ratio of aprotic and protic H atoms). The molecular structure of each adsorbate is indicated in each case, where C, O, aprotic H, and protic H atoms are colored gray, red, blue, and yellow, respectively. Dashed lines in (b) show a linear fit to each data set.

5. Conclusion

To summarize, in this study we have investigated the ^{1}H nuclear spin relaxation characteristics of ten different liquid adsorbates confined within mesoporous silicas with pore sizes between 6 nm and 50 nm. A single relaxation environment was observed for apolar aprotic (cyclohexane), polar aprotic (acetone), and polar protic (water) adsorbates, with their modal T_1/T_2 ratios reflecting increased surface affinity in turn. The different relaxation characteristics associated with the alkyl and hydroxyl groups of seven alcohols (methanol, ethanol, 1-propanol, 1-butanol, 2-propanol, 2-butanol, and ethylene glycol) were clearly distinguished across the full range of material pore sizes examine here, and differences in the modal T_1/T_2 ratios between these moieties related to adsorbate acidity. Both the longitudinal and transverse surface relaxivities of the above adsorbates were evaluated quantitatively via a linear relationship between enhanced relaxation rates and pore structure surface-to-volume ratio, and for the first time, our results demonstrate clear differences in the surface relaxivity values of alkyl and hydroxyl ^{1}H-bearing moieties on the same molecule; longitudinal relaxivity values were found to be universally lower than transverse relaxivity values, while a direct comparison between alkyl and hydroxyl data reveals that the transverse surface relaxivities of adsorbate hydroxyl groups are ≥ 5 times greater than that of the associated alkyl group. Additional trends in transverse surface relaxivity data have also been identified, with alkyl group relaxivities clearly scaling with adsorbate alkyl/hydroxyl ratio.

Overall, our results display a previously unrealized degree of complexity regarding the nuclear spin relaxation characteristics of confined adsorbate liquids. The clear persistence of functional group resolved relaxation phenomena, demonstrated here across a broad range of short chain polar protic hydrocarbon adsorbates (including the first observation of such phenomenon in polyol saturated media), and across the entire range of material pore sizes assessed, is also expected to facilitate new avenues for the characterization of interfacial processes within optically opaque hydroxylated porous materials, and is of direct relevance to the rational design of heterogeneous catalysts systems, where such interfaces are common. Our data, however, further highlight the significant degree of care required in accurately evaluating adsorption phenomena or material structural properties through NMR relaxation analysis. In particular, the realization of significantly different NMR surface relaxivities associated with different ^{1}H-bearing groups on the same adsorbate molecule will be critical in avoiding the erroneous interpretation of relaxation data acquired from porous systems imbibed with complex probe fluids, for example in the evaluation of pore size distributions. In future work we will target an extension of these observations to covalently modified pore surfaces, and to an increased range of functional probe liquids.

Acknowledgements

The authors thank Fuji Silysia Chemical Ltd. (Japan) for providing the mesoporous silica. S. D. would like to thank the Dalian University of Technology for supporting her visit and work at The University of Western Australia. N.R. acknowledges support from the Forrest Research Foundation.

Author Contributions

N.R. designed the research study. S.D. performed the NMR experiments with the aid of N.N.A.L. and analysed the data. L.L. performed the gas sorption experiments. N.R, M.L.J, and E.F.M supervised the research. S.D. and N.R. wrote the manuscript.

Notes

The authors declare no competing financial interests.

References

[1] Yu X, Williams CT. Recent advances in the applications of mesoporous silica in heterogeneous catalysis. Catalysis Science & Technology. 2022;12(19):5765-94.
[2] Sadjadi S, Heravi MM. Current advances in the utility of functionalized SBA mesoporous silica for developing encapsulated nanocatalysts: state of the art. RSC Advances. 2017;7(49):30815-38.
[3] Chen J, Sun C, Huang Z, Qin F, Xu H, Shen W. Fabrication of functionalized porous silica nanocapsules with a hollow structure for high performance of toluene adsorption–desorption. ACS Omega. 2020;5(11):5805-14.
[4] Fatima SS, Borhan A, Ayoub M, Abd Ghani N. Development and progress of functionalized silica-based adsorbents for CO_2 capture. Journal of Molecular Liquids. 2021;338:116913.
[5] Zhang R, Wang X, Liu S, He L, Song C, Jiang X, et al. Discovering inherent characteristics of polyethylenimine-functionalized porous materials for CO_2 capture. ACS Applied Materials & Interfaces. 2019;11(40):36515-24.
[6] Yu J, Corma A, Li Y. Functional porous materials chemistry. Advanced Materials. 2020;32(44):2006277.
[7] Li J, Bhatt PM, Li J, Eddaoudi M, Liu Y. Recent progress on microfine design of metal–organic frameworks: Structure regulation and gas sorption and separation. Advanced Materials. 2020;32(44):2002563.
[8] Maillet B, Sidi-Boulenouar R, Coussot P. Dynamic NMR relaxometry as a simple tool for measuring liquid transfers and characterizing surface and structure evolution in porous media. Langmuir. 2022;38(49):15009-25.
[9] Barrie PJ. Characterization of porous media using NMR methods. Annual Reports on NMR Spectroscopy: Academic Press; 2000. p. 265-316.
[10] Gladden LF, Mitchell J. Measuring adsorption, diffusion and flow in chemical engineering: applications of magnetic resonance to porous media. New Journal of Physics. 2011;13(3):035001.
[11] Song Y-Q. Focus on the physics of magnetic resonance on porous media. New Journal of Physics. 2012;14(5):055017.
[12] Yang M, Chong ZR, Zheng J, Song Y, Linga P. Advances in nuclear magnetic resonance (NMR) techniques for the investigation of clathrate hydrates. Renewable and Sustainable Energy Reviews. 2017;74:1346-60.
[13] Edén M. Probing oxide-based glass structures by solid-state NMR: Opportunities and limitations. Journal of Magnetic Resonance Open. 2023;16-17:100112.
[14] Yi X, Peng Y-K, Chen W, Liu Z, Zheng A. Surface fingerprinting of faceted metal oxides and porous zeolite catalysts by probe-assisted solid-state NMR approaches. Accounts of Chemical Research. 2021;54(10):2421-33.
[15] Brouwer DH, Brouwer CC, Mesa S, Semelhago CA, Steckley EE, Sun MPY, et al. Solid-state 29Si NMR spectra of pure silica zeolites for the International Zeolite Association Database of Zeolite Structures. Microporous and Mesoporous Materials. 2020;297:110000.
[16] Zheng M, Chu Y, Wang Q, Wang Y, Xu J, Deng F. Advanced solid-state NMR spectroscopy and its applications in zeolite chemistry. Progress in Nuclear Magnetic Resonance Spectroscopy. 2024;140-141:1-41.
[17] Brunner E, Rauche M. Solid-state NMR spectroscopy: an advancing tool to analyse the structure and properties of metal–organic frameworks. Chemical Science. 2020;11(17):4297-304.
[18] Klug CA, Swift MW, Miller JB, Lyons JL, Albert A, Laskoski M, et al. High resolution solid state NMR in

paramagnetic metal-organic frameworks. Solid State Nuclear Magnetic Resonance. 2022;120:101811.
[19] Lucier BEG, Chen S, Huang Y. Characterization of metal–organic frameworks: Unlocking the potential of solid-state NMR. Accounts of Chemical Research. 2018;51(2):319-30.
[20] Connolly PRJ, Yan W, Zhang D, Mahmoud M, Verrall M, Lebedev M, et al. Simulation and experimental measurements of internal magnetic field gradients and NMR transverse relaxation times (T_2) in sandstone rocks. Journal of Petroleum Science and Engineering. 2019;175:985-97.
[21] Mitchell J, Chandrasekera TC, Johns ML, Gladden LF, Fordham EJ. Nuclear magnetic resonance relaxation and diffusion in the presence of internal gradients: The effect of magnetic field strength. Physical Review E. 2010;81(2):026101.
[22] Callaghan PT. Translational dynamics and magnetic resonance: Principles of pulsed gradient spin echo NMR. Oxford University Press; 2011.
[23] Price WS. Pulsed-field gradient nuclear magnetic resonance as a tool for studying translational diffusion: Part 1. Basic theory. Concepts in Magnetic Resonance. 1997;9(5):299-336.
[24] Kowalewski J, Maler L. Nuclear spin relaxation in liquids: theory, experiments, and applications. Boca Raton: CRC press, 2017.
[25] Forse AC, Gonzalez MI, Siegelman RL, Witherspoon VJ, Jawahery S, Mercado R, et al. Unexpected diffusion anisotropy of carbon dioxide in the metal–organic framework Zn_2(dobpdc). Journal of the American Chemical Society. 2018;140(5):1663-73.
[26] Witherspoon VJ, Mercado R, Braun E, Mace A, Bachman J, Long JR, et al. Combined nuclear magnetic resonance and molecular dynamics study of methane adsorption in M_2(dobdc) metal–organic frameworks. The Journal of Physical Chemistry C. 2019;123(19):12286-95.
[27] Witherspoon VJ, Yu LM, Jawahery S, Braun E, Moosavi SM, Schnell SK, et al. Translational and rotational motion of C8 aromatics adsorbed in isotropic porous media (MOF-5): NMR studies and MD simulations. The Journal of Physical Chemistry C. 2017;121(28):15456-62.
[28] D'Agostino C, Mitchell J, Gladden LF, Mantle MD. Hydrogen bonding network disruption in mesoporous catalyst supports probed by PFG-NMR diffusometry and NMR relaxometry. The Journal of Physical Chemistry C. 2012;116(16):8975-82.
[29] Forster L, Lutecki M, Fordsmand H, Yu L, D'Agostino C. Tailoring morphology of hierarchical catalysts for tuning pore diffusion behaviour: a rational guideline exploiting bench-top pulsed-field gradient (PFG) nuclear magnetic resonance (NMR). Molecular Systems Design & Engineering. 2020;5(7):1193-204.
[30] Isaacs MA, Robinson N, Barbero B, Durndell LJ, Manayil JC, Parlett CMA, et al. Unravelling mass transport in hierarchically porous catalysts. Journal of Materials Chemistry A. 2019;7(19):11814-25.
[31] Robinson N, D'Agostino C. NMR investigation into the influence of surface interactions on liquid diffusion in a mesoporous catalyst support. Topics in Catalysis. 2020;63(3):319-27.
[32] Yang K, Li M, Ling NNA, May EF, Connolly PRJ, Esteban L, et al. Quantitative tortuosity measurements of carbonate rocks using pulsed field gradient NMR. Transport in Porous Media. 2019;130(3):847-65.
[33] Barberon F, Korb JP, Petit D, Morin V, Bermejo E. Probing the surface area of a cement-based material by nuclear magnetic relaxation dispersion. Physical Review Letters. 2003;90(11):116103.
[34] Robinson N, Nasharuddin R, Luo G, Fourie A, Fridjonsson EO, Johns ML. Pore structure evolution of cemented paste backfill observed with two-dimensional NMR relaxation correlation measurements. Industrial & Engineering Chemistry Research. 2021;60(36):13253-64.
[35] Isaacs MA, Parlett CMA, Robinson N, Durndell LJ, Manayil JC, Beaumont SK, et al. A spatially orthogonal hierarchically porous acid–base catalyst for cascade and antagonistic reactions. Nature Catalysis. 2020;3(11):921-31.
[36] Mensah J, Yan P, Rawal A, Lee AF, Wilson K, Robinson N, et al. Catalytic cracking of 1,3,5-triisopropylbenzene and low-density polyethylene over hierarchical Y zeolites and Al-SBA-15. ChemCatChem. 2024;16(3):e202300884.
[37] Di Carmine G, Forster L, Wang S, Parlett C, Carlone A, D'Agostino C. NMR relaxation time measurements of solvent effects in an organocatalysed asymmetric aldol reaction over silica SBA-15 supported proline. Reaction Chemistry & Engineering. 2022;7(2):269-74.
[38] Silletta EV, Velasco MI, Gomez CG, Strumia MC, Stapf S, Mattea C, et al. Enhanced surface interaction of water confined in hierarchical porous polymers induced by hydrogen bonding. Langmuir. 2016;32(29):7427-34.
[39] Suekuni MT, Allgeier AM. Correlating surface chemistry to surface relaxivity via TD-NMR studies of polymer particle suspensions. JACS Au. 2023;3(10):2826-34.
[40] D'Agostino C, Bräuer P. Exploiting enhanced paramagnetic NMR relaxation for monitoring catalyst preparation using T_1–T_2 NMR correlation maps. Reaction Chemistry & Engineering. 2019;4(2):268-72.
[41] Forster L, Kashbor MMM, Railton J, Chansai S, Hardacre C, Conte M, et al. Low-field 2D NMR relaxation and DRIFTS studies of glucose isomerization in zeolite Y: New insights into adsorption effects on catalytic performance. Journal of Catalysis. 2023;425:269-85.
[42] Mitchell J, Broche LM, Chandrasekera TC, Lurie DJ, Gladden LF. Exploring surface interactions in catalysts using Low-Field nuclear magnetic resonance. The Journal of Physical Chemistry C. 2013;117(34):17699-706.
[43] Zheng Q, Williams J, van Thiel LR, Elgersma SV, Mantle MD, Sederman AJ, et al. Operando magnetic resonance

imaging of product distributions within the pores of catalyst pellets during Fischer–Tropsch synthesis. Nature Catalysis. 2023;6(2):185-95.
[44] McDonald PJ, Korb JP, Mitchell J, Monteilhet L. Surface relaxation and chemical exchange in hydrating cement pastes: A two-dimensional NMR relaxation study. Physical Review E. 2005;72(1):011409.
[45] Song Y-Q, Kausik R. NMR application in unconventional shale reservoirs – A new porous media research frontier. Progress in Nuclear Magnetic Resonance Spectroscopy. 2019;112-113:17-33.
[46] McDonald PJ, Mitchell J, Mulheron M, Monteilhet L, Korb J-P. Two-dimensional correlation relaxation studies of cement pastes. Magnetic Resonance Imaging. 2007;25(4):470-3.
[47] Yang K, Conolly PRJ, Liu L, Yang X, Robinson N, Li M, et al. Quantitative characterization of methane adsorption in shale using low-field NMR. Journal of Natural Gas Science and Engineering. 2022;108:104847.
[48] D'Agostino C, Mitchell J, Mantle MD, Gladden LF. Interpretation of NMR relaxation as a tool for characterising the adsorption strength of liquids inside porous materials. Chemistry – A European Journal. 2014;20(40):13009-15.
[49] Robinson N, Robertson C, Gladden LF, Jenkins SJ, D'Agostino C. Direct correlation between adsorption energetics and nuclear spin relaxation in a liquid-saturated catalyst material. ChemPhysChem. 2018;19(19):2472-9.
[50] Robinson N, Bräuer P, York APE, D'Agostino C. Nuclear spin relaxation as a probe of zeolite acidity: a combined NMR and TPD investigation of pyridine in HZSM-5. Physical Chemistry Chemical Physics. 2021;23(33):17752-60.
[51] Krzyżak AT, Habina I. Low field ^{1}H NMR characterization of mesoporous silica MCM-41 and SBA-15 filled with different amount of water. Microporous and Mesoporous Materials. 2016;231:230-9.
[52] Song YQ, Venkataramanan L, Hürlimann MD, Flaum M, Frulla P, Straley C. T_1–T_2 correlation spectra obtained using a fast two-dimensional laplace inversion. Journal of Magnetic Resonance. 2002;154(2):261-8.
[53] Weber D, Mitchell J, McGregor J, Gladden LF. Comparing strengths of surface interactions for reactants and solvents in porous catalysts using two-dimensional NMR relaxation correlations. The Journal of Physical Chemistry C. 2009;113(16):6610-5.
[54] Robinson N, May EF, Johns ML. Low-Field functional group resolved nuclear spin relaxation in mesoporous silica. ACS Applied Materials & Interfaces. 2021;13(45):54476-85.
[55] D'Agostino C, York APE, Bräuer P. Host-guest interactions and confinement effects in HZSM-5 and chabazite zeolites studied by low-field NMR spin relaxation. Materials Today Chemistry. 2022;24:100901.
[56] Robinson N, D'Agostino C, Johns ML. Functional group resolved NMR relaxation of 3-carbon adsorbates in mesoporous alumina. Magnetic Resonance Letters. 2023;3(3):248-55.
[57] Ward-Williams J, Korb JP, Gladden LF. Insights into functionality-specific adsorption dynamics and stable reaction intermediates using fast field cycling NMR. The Journal of Physical Chemistry C. 2018;122(35):20271-8.
[58] Ward-Williams J, Korb J-P, Rozing L, Sederman AJ, Mantle MD, Gladden LF. Characterizing solid–liquid interactions in a mesoporous catalyst support using variable-temperature fast field cycling NMR. The Journal of Physical Chemistry C. 2021;125(16):8767-78.
[59] Ward-Williams J, Gladden LF. Insights into adsorption behaviour of binary liquid mixtures in porous media using fast field cycling NMR. Magnetic Resonance Imaging. 2019;56:57-62.
[60] Liu G, Li Y, Jonas J. Confined geometry effects on reorientational dynamics of molecular liquids in porous silica glasses. The Journal of Chemical Physics. 1991;95(9):6892-901.
[61] Brownstein KR, Tarr CE. Importance of classical diffusion in NMR studies of water in biological cells. Physical Review A. 1979;19(6):2446-53.
[62] Keating K, Knight R. The effect of spatial variation in surface relaxivity on nuclear magnetic resonance relaxation rates. GEOPHYSICS. 2012;77(5):E365-E77.
[63] Kinn BE, Myers TR, Allgeier AM. Surface enhanced nuclear magnetic resonance relaxation mechanisms and their significance in chemical engineering applications. Current Opinion in Chemical Engineering. 2019;24:115-21.
[64] Stingaciu LR, Weihermüller L, Haber-Pohlmeier S, Stapf S, Vereecken H, Pohlmeier A. Determination of pore size distribution and hydraulic properties using nuclear magnetic resonance relaxometry: A comparative study of laboratory methods. Water Resources Research. 2010;46(11):W11510.
[65] Jaeger F, Bowe S, Van As H, Schaumann GE. Evaluation of ^{1}H NMR relaxometry for the assessment of pore-size distribution in soil samples. European Journal of Soil Science. 2009;60(6):1052-64.
[66] Hinedi ZR, Kabala ZJ, Skaggs TH, Borchardt DB, Lee RWK, Chang AC. Probing soil and aquifer material porosity with nuclear magnetic resonance. Water Resources Research. 1993;29(12):3861-6.
[67] Olajire AA. Synthesis of bare and functionalized porous adsorbent materials for CO_2 capture. Greenhouse Gases: Science and Technology. 2017;7(3):399-459.
[68] D'Agostino C, Bräuer P, Zheng J, Robinson N, York APE, Song L, et al. Adsorbate/adsorbent interactions in microporous zeolites: mechanistic insights from NMR relaxation and DFT calculations. Materials Today Chemistry. 2023;29:101443.
[69] Mitchell J, Chandrasekera TC. Understanding generalized inversions of nuclear magnetic resonance transverse relaxation time in porous media. The Journal of Chemical Physics. 2014;141(22):224201.
[70] McCall KR, Johnson DL, Guyer RA. Magnetization evolution in connected pore systems. Physical Review B. 1991;44(14):7344-55.

[71] Washburn KE, Eccles CD, Callaghan PT. The dependence on magnetic field strength of correlated internal gradient relaxation time distributions in heterogeneous materials. Journal of Magnetic Resonance. 2008;194(1):33-40.
[72] Korb J-P. Multiscale nuclear magnetic relaxation dispersion of complex liquids in bulk and confinement. Progress in Nuclear Magnetic Resonance Spectroscopy. 2018;104:12-55.
[73] Robinson N, Nasharuddin R, Fridjonsson EO, Johns ML. NMR surface relaxivity in a time-dependent porous system. Physical Review Letters. 2023;130(12):126204.
[74] Duschl M, Galvosas P, Brox TI, Pohlmeier A, Vereecken H. In situ determination of surface relaxivities for unconsolidated sediments. Water Resources Research. 2015;51(8):6549-63.
[75] Penrose C, Steiner P, Gladden LF, Sederman AJ, York APE, Bentley M, et al. A simple liquid state ^{1}H NMR measurement to directly determine the surface hydroxyl density of porous silica. Chemical Communications. 2021;57(95):12804-7.
[76] Bardenhagen I, Dreher W, Fenske D, Wittstock A, Bäumer M. Fluid distribution and pore wettability of monolithic carbon xerogels measured by ^{1}H NMR relaxation. Carbon. 2014;68:542-52.
[77] Mitchell J, Chandrasekera TC, Gladden LF. Numerical estimation of relaxation and diffusion distributions in two dimensions. Progress in Nuclear Magnetic Resonance Spectroscopy. 2012;62:34-50.
[78] Tikhonov AN, Arsenin VIA. Solutions of Ill-posed problems: Winston, 1977.
[79] Golub GH, Heath M, Wahba G. Generalized cross-validation as a method for choosing a good ridge parameter. Technometrics. 1979;21(2):215-23.
[80] Mitchell J, Graf von der Schulenburg DA, Holland DJ, Fordham EJ, Johns ML, Gladden LF. Determining NMR flow propagator moments in porous rocks without the influence of relaxation. Journal of Magnetic Resonance. 2008;193(2):218-25.
[81] Reichardt C. Solvents and solvent effects in organic chemistry. Weinheim, Germany: Wiley-VCH, 2003.
[82] Robinson N. Nuclear spin relaxation and diffusion studies of adsorption and dynamics at the catalyst-liquid interface. Cambridge, UK: University of Cambridge, 2020.
[83] Faux DA, McDonald PJ. Explicit calculation of nuclear-magnetic-resonance relaxation rates in small pores to elucidate molecular-scale fluid dynamics. Physical Review E. 2017;95(3):033117.
[84] D'Orazio F, Tarczon JC, Halperin WP, Eguchi K, Mizusaki T. Application of nuclear magnetic resonance pore structure analysis to porous silica glass. Journal of Applied Physics. 1989;65(2):742-51.
[85] Korb JP. Nuclear magnetic relaxation of liquids in porous media. New Journal of Physics. 2011;13(3):035016.